JOURNAL OF MATERIALS SCIENCE 26 (1991) 1821 – 1826

Orientation preference and fractal character of short fatigue cracks in a weld metal

YOUSHI HONG, YONGHUA LU, ZHEMIN ZHENG
Institute of Mechanics, Academia Sinica, Beijing 100080, People's Republic of China

Short fatigue crack behaviour in a weld metal has been further investigated. The Schmid factor and the fractal dimension of short cracks on iso-stress specimens subjected to reversed bending have been determined and then applied to account for the distribution and orientation characteristics of short fatigue cracks. The result indicates that the orientation preference of short cracks is attributed to the large values of Schmid factor at relevant grains. The Schmid factors of most slip systems, which produced short cracks, are less than or equal to 0.4. Crack length measurements reveal that short crack path, compared to that of long crack, possesses a more stable and relatively larger value of fractal dimension. This is regarded as one of the typical features of short cracks.

1. Introduction

The initiation and propagation behaviour of short fatigue cracks have been extensively studied during the past 10 years. Many investigations have demonstrated that short cracks may initiate at inclusions or second phase particles in aluminium alloys [1, 2] and structural steels [3], or may generate from slip bands in weld metal [4], nickel [5], and Ni–Cu alloy [6]. The growth of short cracks has been reported as an intermittent, decelerating and accelerating pattern [7, 8]. In most cases, the size of short cracks is comparable to the relevant microstructural element, e.g. grain size, inclusion spacing etc., thus the behaviour of short cracks is greatly influenced by the microstructure of the material investigated.

On the other hand, the fractal dimension concept has been introduced into the area of fracture research during the recent years. The fracture surface of a maraging steel is found to be fractal in nature and the fractal dimension of the surface correlates well with the impact toughness [9]. According to the theory of self-similarity, Pande *et al.* [10] proposed a simple definition of fractal dimension D_F

$$L = L_0 \eta^{-(D_F - D)} \quad (1)$$

where L is the measured length, area etc., η the measuring unit, L_0 a constant and D the topological dimension. For a straight line, $D_F = D = 1$. Equation 1 was used to obtain an approximate relationship between fractal dimension and dynamic tear energy of a titanium alloy.

The present study attempts to investigate the distribution and orientation characteristics of short cracks in the specially designed triangular specimens subjected to reversed bending, in the light of the Schmid factor concept and fractal dimension theory.

2. Procedure

2.1. Material and fatigue testing

The experimental material is a weld metal with the chemical composition of (wt %) C0.12, Si0.55, Mn0.97, P0.025, S0.012, O0.032, N0.011 and Fe balance. Specimen blanks were austenitized at 925 °C and then air cooled. The normalized microstructure consists of ferrite and pearlite. The average ferrite grain size is 22 μm and the pearlite percentage is 16%; both were obtained by optical microscopy. The yield stress σ_y, obtained by uniaxial tensile testing, is 310 MPa. The triangular specimen shown in Fig. 1 was used in the fatigue testing, for which the surface tensile stress σ_{max} remains constant over the gauge length when the specimen is subjected to a given loading. The design and preparation details of the specimen have been described elsewhere [4, 11].

Fatigue testing was carried out by using a vibration machine at a frequency between 10 and 12 Hz for stress ratio $R = -1$ and $\sigma_{max} = 0.8$ to $1.2\sigma_y$. The cycling was periodically interrupted and the specimen was observed by a Polyvarmet microscope with POL illumination. The photographs taken tracked the initiation and development process of short cracks.

2.2. Schmid factor determination

After the fatigue testing, some specimens were longitudinally sectioned, which were then mounted, ground and polished. Such profile samples were examined by optical and SEM techniques. The angle between a short crack and specimen surface (i.e. tensile stress direction), which is denoted as β in Fig. 2, was measured. On the other hand, α, also shown in Fig. 2, was defined as the angle between a short crack and tensile stress direction on the specimen surface. It is obvious that a developed short crack can be observed both on

0022–2461/91 $03.00 + .12

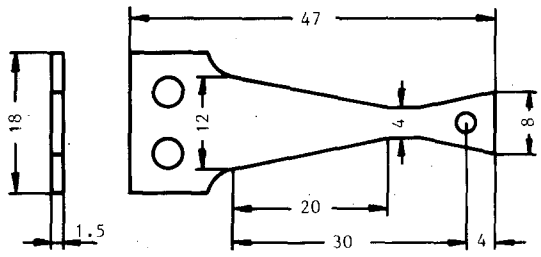

Figure 1 Schematic of triangular specimen (dimensions in mm).

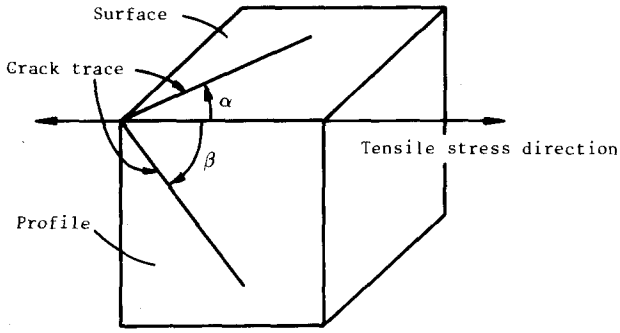

Figure 2 Schematic of crack traces on specimen surface and profile.

the surface and the profile of specimen, and that a pair of α and β describes the orientation of a crack. Since, in the present case, short cracks originate from slip bands, the plane constructed by a set of α and β corresponds to a slip plane with a unit vector $\boldsymbol{r}$ directed along its normal. If one assumes that slip operates along the direction observed in the profile section, then one can calculate the Schmid factor, M, of each pair of α and β, using the following equation

$$M = \cos\phi\cos\lambda = \frac{\boldsymbol{r}\cdot\boldsymbol{T}}{|\boldsymbol{r}||\boldsymbol{T}|}\cos\beta \qquad (2)$$

where φ is the angle between the normal to the slip plane and the tensile stress direction, λ the angle that the slip direction makes with the tensile axis, and $\boldsymbol{T}$ the unit vector of tensile stress direction.

2.3. Fractal dimension determination

The lengths of developed short cracks on a specimen surface, which had experienced more than 10^5 cycles of loading, were also measured using the microscope with different measuring scales, η_m, ranging from 3 to 3000 μm. To normalize the measuring scale, we take

$$\eta = \frac{\eta_m}{\eta_0} \qquad (3)$$

where η_0 is the average grain diameter, then, from Equation 1, we have

$$\log L = \log L_0 - (D_F - D)\log\frac{\eta_m}{\eta_0} \qquad (4)$$

If log L and log (η_m/η_0) are linearly related, then a self-similarity pattern exists. The fractal dimension of short crack path can thus be obtained from the slope of the linear relation. In order to make a comparison between short and long cracks, we also measured the fractal dimension of the long crack path, using the same method, as on pre-cracked three-point bend specimens [12].

3. Results and discussions

3.1. Distribution and orientation of short cracks

The observations from specimen surfaces at different fatigue testing intervals revealed that short cracks originate from slip bands of ferrite grains and the number of short cracks gradually increases with fatigue cycles (Fig. 3a to d). Macroscopically, the distribution of short cracks at initiation, within the specimen gauge length where a constant surface tensile stress prevails, is nearly uniform. Microscopically, however, short cracks distribute quite unevenly among different ferrite grains. This has two implications. First, at the early stage, short cracks appear only in a few ferrite grains, the orientation of which tends to be perpendicular to the surface tensile stress or α tends to π/2 (Fig. 3b). Subsequently, new cracks initiate both in the grains with prior cracks and in some others without previous cracking. The later formed short cracks lie in directions gradually deviating from the axis perpendicular to the tensile stress. Eventually, the distribution of angle α covers a range from 90° to 45° (Fig. 3c and d). Secondly, even though a specimen has experienced more than 10^5 cycles at $\sigma_{max} = 1.2\sigma_y$, and short cracks have become densely distributed with a few of them across several ferrite grains, some ferrite domains remain undamaged with not a single short crack appearing in such grains (Fig. 4).

The examinations from profile samples, on the other hand, indicated that the surface cracks, with their length comparable to or less than the corresponding ferrite grain size, can hardly be identified in the depth direction, which implies that although they can be recognized by their two banks on the surface, such short cracks are very shallow in depth, obviously much less than grain size. This is mainly due to prevalence of the largest stress on the specimen surface and it diminishes to zero at the mid-section. Only those main cracks, each with a length of several grain sizes, can be observed on the profile with their depths varying from 10 to 100 μm (Fig. 5). The angle between a crack and specimen surface, β, was measured from SEM photographs. The result is shown in Fig. 6.

To sum up the results described above, of the crack orientation on the surface and profile, we have, respectively

$$\frac{(2n+1)\pi}{2} - \frac{\pi}{4} \leqslant \alpha \leqslant \frac{(2n+1)\pi}{2} + \frac{\pi}{4}, \quad n = 0,1 \qquad (5)$$

and

$$\frac{(2n+1)\pi}{4} - \frac{\pi}{12} \leqslant \beta \leqslant \frac{(2n+1)\pi}{4} + \frac{\pi}{12}, \quad n = 0,1 \qquad (6)$$

The result of Schmid factor estimation was obtained

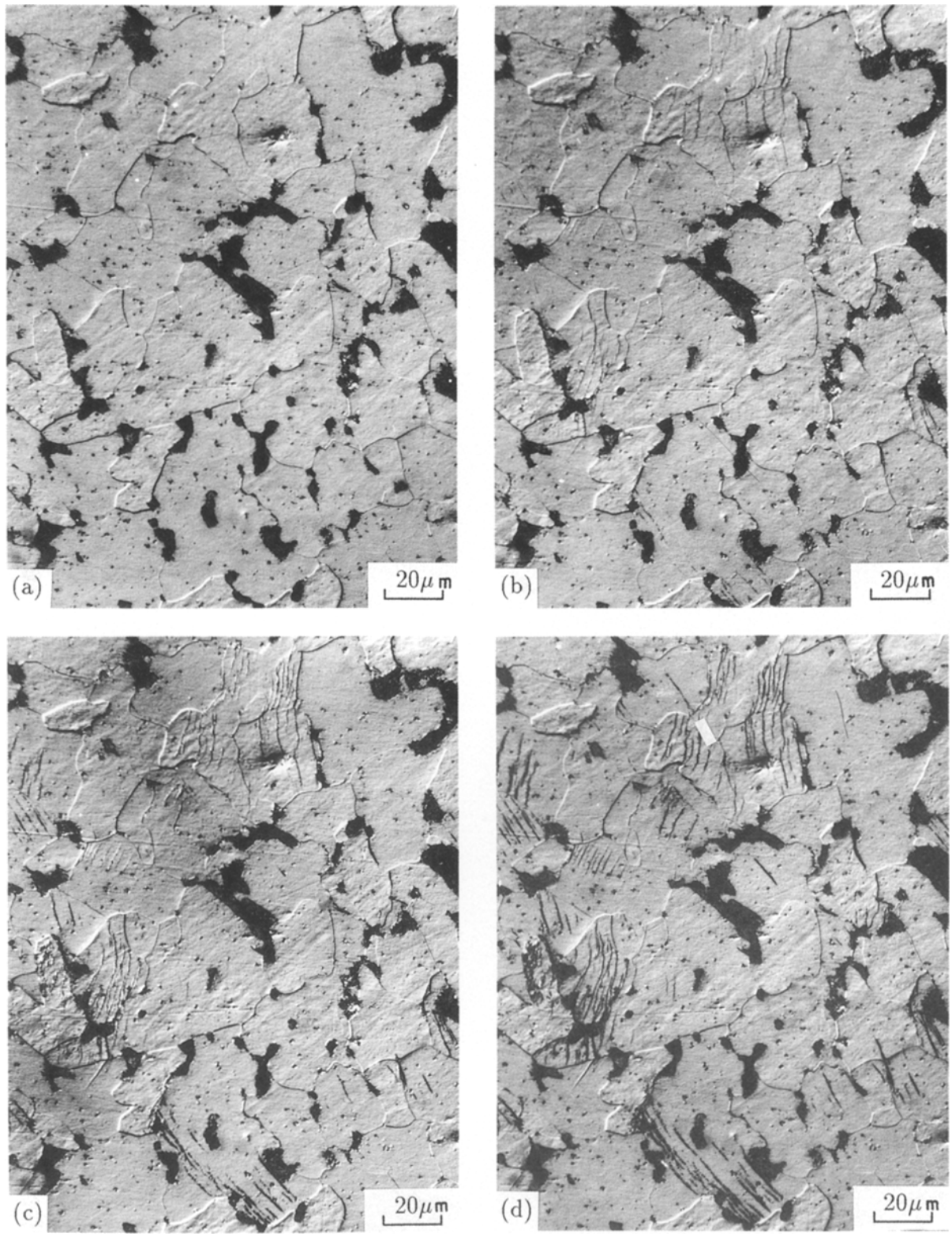

Figure 3 Photos of the same field showing the development of short fatigue cracks on an etched specimen at $\sigma_{max} = 1.2\sigma_y$ (transverse axis parallel to tensile stress). (a) $N = 0$, (b) $N = 6000$, (c) $N = 30\,000$, (d) $N = 61\,000$, where N is number of fatigue cycles.

by Equation 2. From the symmetry of crack orientation, we take $\pi/6 \leqslant \alpha \leqslant \pi/2$ and $\pi/8 \leqslant \beta \leqslant 3\pi/8$ in the estimation. Fig. 7 shows the three-dimensional construction and Fig. 8 the contour line of the result. Only when $\alpha = \pi/2$, the value of M, i.e. the Schmid factor is symmetrical with β and reaches its maximum when $\beta = \pi/4$. The value of M declines unsymmetrically along the directions of $\pi/4 < \beta < \pi/4$ and $\alpha < \pi/2$, with a faster decreasing rate towards the side of $\beta > \pi/4$. The larger the value of the Schmid factor, the more prone to slip of the relevant system. This result gives explicit illustration about the fact that α tends towards $\pi/2$ for the earlier formed short cracks. Figs 7 and 8 also indicate that the orientation of most short cracks was located within the Schmid factor range of $M \geqslant 0.4$. The outline shown in Fig. 9, which is the back view of Fig. 7, is consistent with the distribution pattern of Fig. 6, indicating that the distribution of

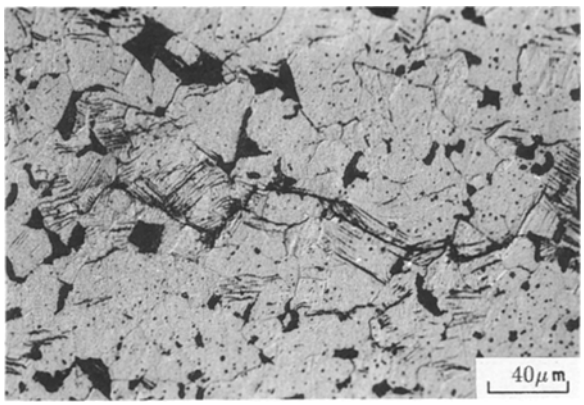

Figure 4 A main crack across several ferrite grains after $N = 230\,000$ at $\sigma_{max} = 1.2\sigma_y$ (vertical axis parallel to tensile stress).

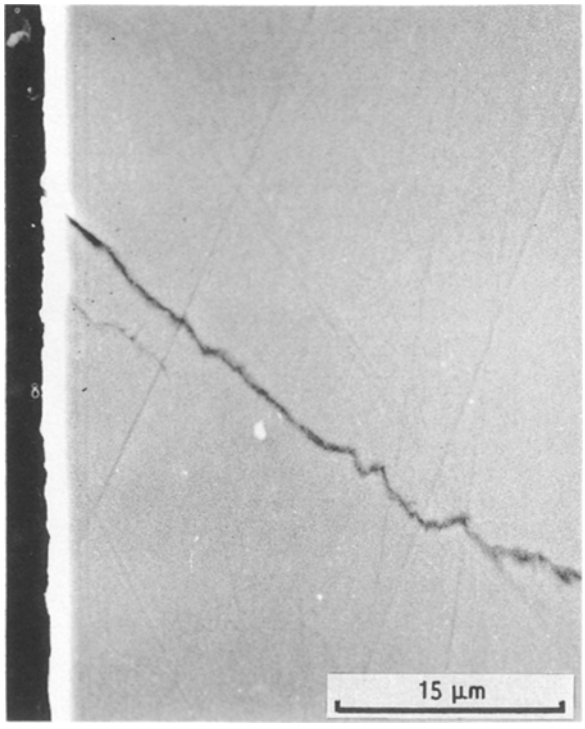

Figure 5 Two cracks on a profile section (the left edge is the specimen surface and the vertical axis is parallel to the tensile stess).

crack orientation is closely related to the distribution of the Schmid factor.

3.2. Fractal dimension of short crack path

Figs 10 and 11 show the results of short crack length measurements. It is found that, within the scale range of

$$0.15 \leqslant \eta \leqslant 45 \qquad (7)$$

or

$$3\ \mu m \leqslant \eta_m \leqslant 1000\ \mu m$$

a very good linear trend exists between $\log L$ and $\log \eta$ (Fig. 10). Five groups of data of Fig. 10 were linear-regressed and the fractal dimension of the short crack path, D_{Fs}, was obtained

$$D_{Fs} - D = 0.055 \pm 0.002$$

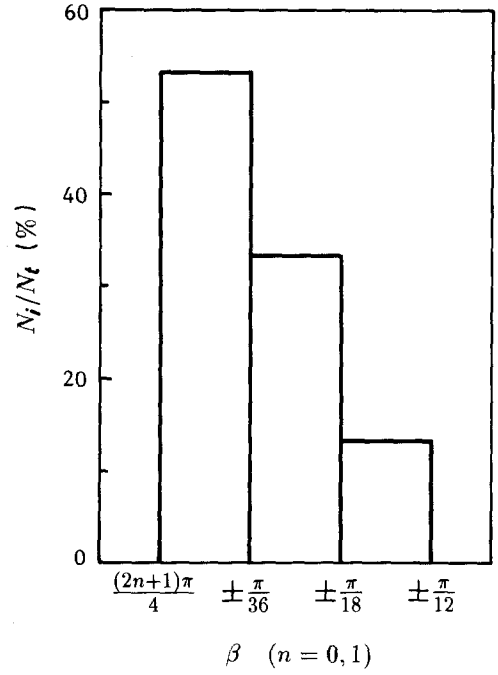

Figure 6 Distribution of angle β, where N_i is the number of cracks at β_i and N_t the total number of cracks.

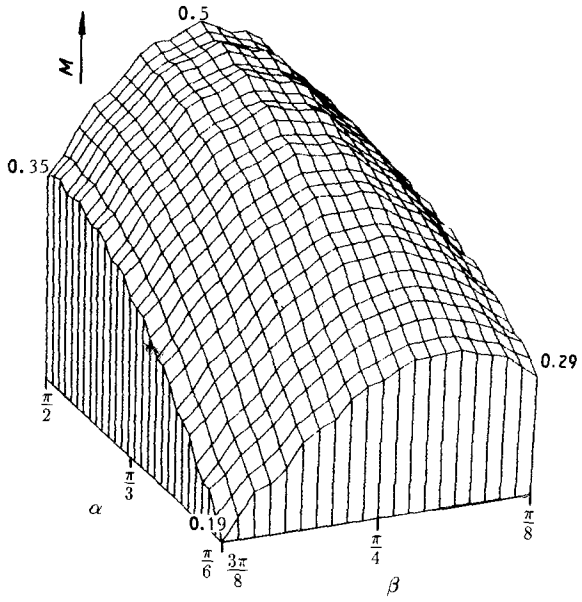

Figure 7 Three-dimensional construction of Schmid factor distribution.

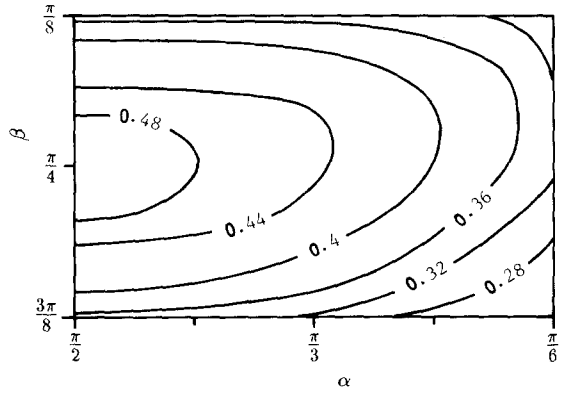

Figure 8 Contour line of the Schmid factor distribution, the numbers show the values of Schmid factor.

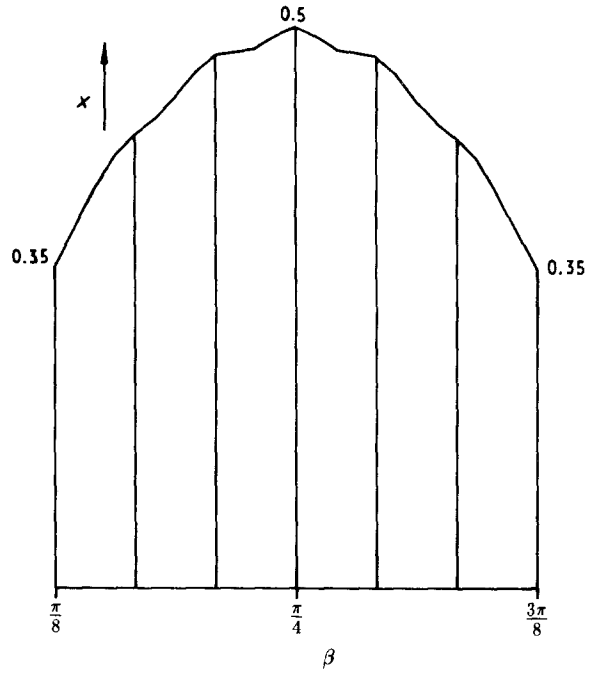

Figure 9 Schmid factor distribution at $\alpha = \pi/2$ and $\pi/8 \leqslant \beta \leqslant 3\pi/8$.

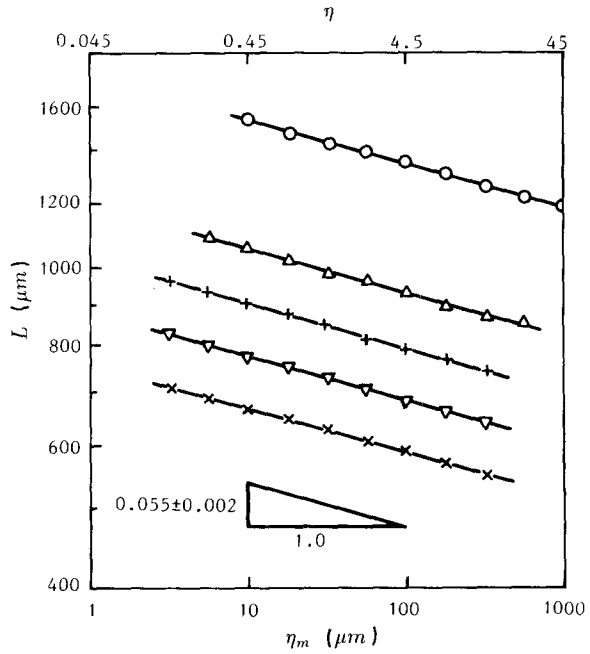

Figure 10 Variation of short crack length as a function of measuring scale ($\eta_m \leqslant 1000$ μm).

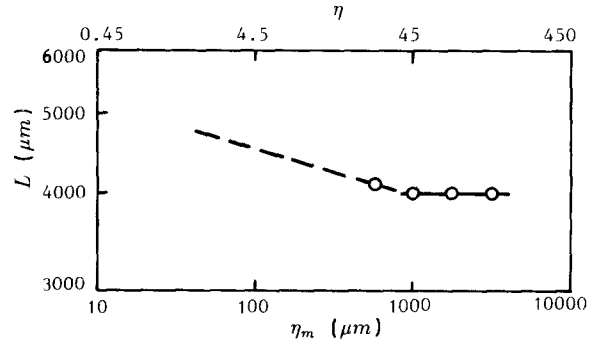

Figure 11 Short crack length being constant with measuring scale when $\eta_m > 1000$ μm.

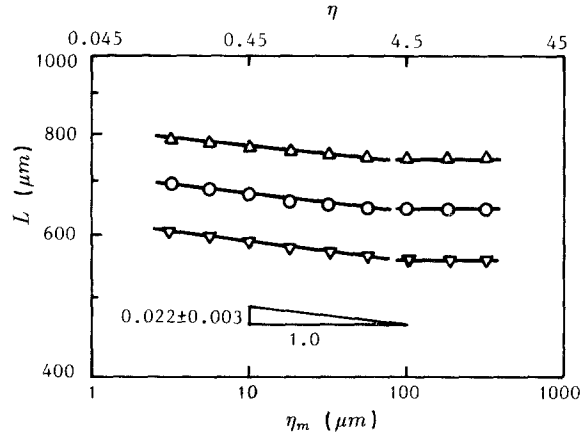

Figure 12 Variation of long crack length as a function of measuring scale.

or

$$D_{Fs} = 1.055 \pm 0.002 \quad (8)$$

for which the correlation coefficients $r \geqslant 0.997$. This result reveals that a short crack path possesses an evident and stable fractal feature within a definite scale range. Beyond this range, however, the value of L keeps almost constant when η becomes larger (Fig. 11).

On the other hand, the length measurements of long cracks (Fig. 12) show a clear difference in fractal character between the two types of cracks. For a long crack path, only when

$$0.15 \leqslant \eta \leqslant 4.5 \quad (9)$$

or

$$3\ \mu m \leqslant \eta_m \leqslant 100\ \mu m$$

does a relatively smaller value of fractal dimension exist. Beyond the range, L keeps constant as η increases. Also using the linear regression method, we obtain

$$D_{Fl} - D = 0.022 \pm 0.003$$

or

$$D_{Fl} = 1.022 \pm 0.003 \quad (10)$$

where the subscipt 1 denotes a long crack and the correlation coefficients $r \geqslant 0.990$.

Short cracks originate from slip bands and the grain boundaries act as the dominant barriers against crack advance, thus a developed short crack always deflects at grain boundaries (Fig. 4), which makes the path of a short crack more wavy than that of a long crack. This distinct feature of short cracks can be expressed by a substantially large value of fractal dimension it possessed.

4. Conclusions

The conclusions are as follows.

1. The distribution and orientation preference of short fatigue cracks is associated to the Schmid factor of relevant grains. The Schmid factors of most slip

systems which produced short cracks are greater than or equal to 0.4.

2. Short crack path possesses a stable and substantially large value of fractal dimension, which is one of the distinct characteristics of short cracks.

Acknowledgement

This paper is supported by the Chinese Academy of Sciences under Special Grant No. 87-052.

References

1. J. LANKFORD, *Fatigue Engng Mater. Struct.* **5** (1982) 233.
2. W. L. MORRIS, *Met. Trans.* **10A** (1979) 5.
3. E. C. PEREZ and M. W. BROWN, *Fatigue Frac. Engng Mater. Struct.* **9** (1986) 15.
4. Y. HONG, Y. LU and Z. ZHENG, *ibid.* **12** (1989) 323.
5. C. E. PRICE, *ibid.* **11** (1988) 483.
6. C. E. PRICE and G. W. HENDERSON, *ibid.* **11** (1988) 493.
7. K. TANAKA, M. HOJO and Y. NAKAI, ASTM STP 811 (American Society for Testing and Materials, Philadelphia, 1983) p. 207.
8. C. W. BROWN and M. A. HICKS, *Fatigue Engng Mater. Struct.* **6** (1983) 67.
9. B. B. MANDELBROT, D. E. PASSOJA and A. J. PAULLAY, *Nature* **308** (1984) 721.
10. C. S. PANDE, L. E. RICHARDS, N. LOUAT, B. D. DEMPSEY and A. J. SCHWOEBLE, *Acta Metall.* **35** (1987) 1633.
11. Y. HONG, Y. LU and Z. ZHENG, *Acta Metall. Sinica (English Edition)* **A3** (1990) 276.
12. Y. LU and Y. HONG, Internal research report.

Received 23 January
and aceepted 3 July 1990